Article

A Homoleptic Molybdenum(IV) Enolate Complex: Synthesis, Molecular and Electronic Structure, and NCN Group Transfer To Form a Terminal Cyanoimide of Molybdenum(VI)

Han Sen Soo, Joshua S. Figueroa, and Christopher C. Cummins

J. Am. Chem. Soc., **2004**, 126 (36), 11370-11376• DOI: 10.1021/ja0472533 • Publication Date (Web): 20 August 2004

J|A|C|S
ARTICLES
Published on Web 08/20/2004

A Homoleptic Molybdenum(IV) Enolate Complex: Synthesis, Molecular and Electronic Structure, and NCN Group Transfer To Form a Terminal Cyanoimide of Molybdenum(VI)

Han Sen Soo, Joshua S. Figueroa, and Christopher C. Cummins*

Contribution from the Department of Chemistry, Room 2-227, Massachusetts Institute of Technology, 77 Massachusetts Avenue, Cambridge, Massachusetts 02139-4307

Received May 11, 2004; E-mail: ccummins@mit.edu

Abstract: A monomeric molybdenum(IV) tetrakis enolate complex $Mo(OC[Ad]Mes)_4$, **1**, where Ad = 2-adamantylidene and Mes = $2,4,6\text{-}Me_3C_6H_2$, has been synthesized and characterized structurally by X-ray diffraction, chemically through NCN group-transfer reactivity, and computationally to investigate the origins of the observed structure that is intermediate between tetrahedral and square planar. No prior examples of $Mo(OR)_4$ have been structurally characterized despite having been the subject of both experimental and theoretical interest. Complex **1** has a singlet ground state and thus a metal-based lone pair of electrons. The latter has been visualized with the aid of the electron localization function (ELF) and appears as a two-bladed propeller with D_{2d} symmetry. Complex **1** makes a simple 1:1 adduct with *t*-BuNC that is trigonal bipyramidal with an axial isocyanide as demonstrated by X-ray crystallography. This trigonal bipyramidal 1:1 adduct has a triplet ground state and provides a model for the way in which **1** interacts with NCN group donor *dbabh*CN prior to NCN group transfer to form the terminal cyanoimide complex **1**-NCN. The calculated Mo−N bond dissociation enthalpy for **1**-NCN is 104 kcal mol^{-1}, 30 kcal mol^{-1} greater than that for the corresponding dissociation of NCN from cyanophosphiniminato $NCNPMe_3$.

Introduction

Complexes with the general formula $Mo(OR)_4$ represent an interesting type of reactive metal fragment due to the combination of coordinative unsaturation,[1] a d^2 electron count, and the absence of π-acid ligands. While it appears that no $Mo(OR)_4$ complex has to date been structurally characterized, the green-brown compound $Mo(O\text{-}t\text{-}Bu)_4$ is known.[2,3] The preferred coordination geometry for $Mo(OR)_4$ systems has been predicted on theoretical grounds to be square-planar.[4] This is in concert with the known, essentially square-planar structure of $W(OAr)_4$ ($Ar = 2,6\text{-}C_6H_3\text{-}i\text{-}Pr_2$).[5,6] Originally, it was thought that the steric demands of the alkoxide substituent in $Mo(OR)_4$ (R = *t*-Bu, $CMeEt_2$, CEt_3, or 1-adamantyl) prevented these derivatives from adopting the preferred square-planar arrangement, with the ensuing pseudo-tetrahedral geometry rendering the complexes paramagnetic.[2] More recent studies of $Mo(O\text{-}t\text{-}Bu)_4$, however, suggest that this derivative is diamagnetic,[3] consistent with a geometry approaching square planar.

Recently, we reported the design and synthesis of a bulky enolate ligand (OC[Ad]Mes, where Ad = 2-adamantylidene and Mes = $2,4,6\text{-}C_6H_3Me_2$; see Figure 1) intended to stabilize metal centers having a low coordination number.[7] In the present contribution, we describe the synthesis and structural characterization of the homoleptic molybdenum(IV) complex $Mo(OC[Ad]Mes)_4$, **1**. Also described herein are attributes of the electronic structure of **1** as investigated using density functional theory (DFT) calculations, as well as preliminary reactivity studies including isocyanide binding and an NCN group-transfer reaction.

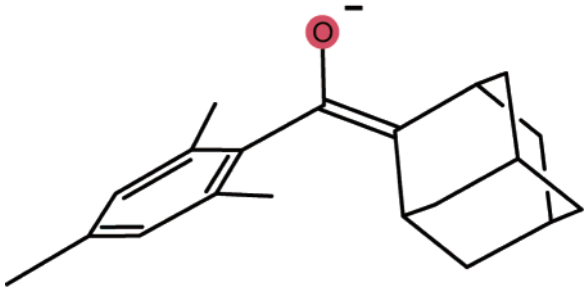

Figure 1. The enolate ligand $^-OC[Ad]Mes$.

Results and Discussion

Synthesis of Complex 1. Reactions of the potassium salt $K(OC[Ad]Ar)$[7] with both molybdenum(III) and molybdenum(IV) chlorides were investigated. In the case of the K(OC[Ad]-

(1) Strauss, S. H. *Chemtracts: Inorg. Chem.* **1994**, *6*, 1−13.
(2) Chisholm, M. H.; Reichert, W. W.; Thornton, P. *J. Am. Chem. Soc.* **1978**, *100*, 2744−2748.
(3) Stoffelbach, F.; Saurenz, D.; Poli, R. *Eur. J. Inorg. Chem.* **2001**, 2699−2703.
(4) Cayton, R. H.; Chisholm, M. H.; Clark, D. L.; Hammond, C. E. *J. Am. Chem. Soc.* **1989**, *111*, 2751−2755.
(5) Listemann, M. L.; Dewan, J. C.; Schrock, R. R. *J. Am. Chem. Soc.* **1985**, *107*, 7207−7208.
(6) Listemann, M. L.; Schrock, R. R.; Dewan, J. C.; Kolodziej, R. M. *Inorg. Chem.* **1988**, *27*, 264−271.
(7) Soo, H. S.; Diaconescu, P. L.; Cummins, C. C. *Organometallics* **2004**, *23*, 498−503.

10.1021/ja0472533 CCC: $27.50

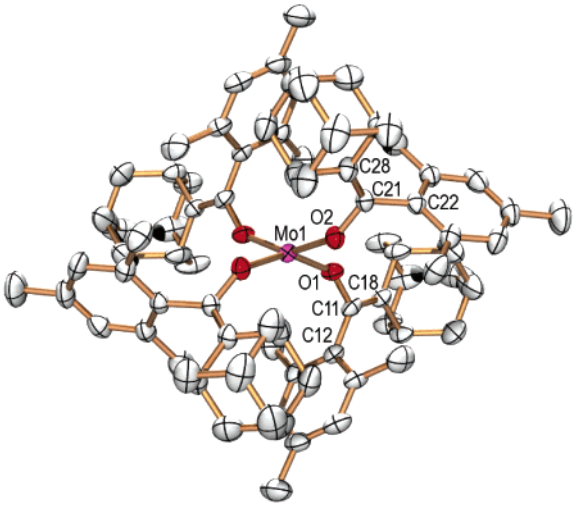

Figure 2. ORTEP[9] representation of **1** (crystallographic C_2 axis normal to page) with thermal ellipsoids drawn at the 50% probability level. Not shown is an Et_2O molecule of crystallization. Selected interatomic distances (Å) and angles (deg): Mo1−O1, 1.866(3); Mo1−O2, 1.869(3); O1−Mo1−O2′, 150.69(12); O1−Mo1−O2, 94.73(11); C11−O1−Mo1, 147.7(3); C21−O2−Mo1, 145.6(3).

Ar)/$MoCl_3(THF)_3$ reaction system, **1** was obtained serendipitously and in low yield (12%), so a purposeful synthesis of **1** was developed. Treatment of $MoCl_4(THF)_2$ with 4.1 equiv of K(OC[Ad]Ar) was found to give **1** in 37% yield, after purification, on a reaction scale that affords ca. 3 g of the desired product. Pure **1** is a yellow-green solid, soluble in aromatic hydrocarbon solvents but essentially insoluble in hexane or diethyl ether. The proton NMR spectrum in C_6D_6 of diamagnetic **1** has a characteristic broad signal at $\delta = 5.16$ ppm assigned, with the aid of DEPT, HETCOR, and COSY experiments,[8] to one of the two allylic methine protons present on the 2-adamantylidene cage. At 25 °C in C_6D_6 solution, complex **1** exhibits a single set of enolate ligand NMR resonances. The appearance and chemical shift range for the ^1H and ^{13}C NMR signals associated with **1** are consistent with its being a diamagnetic enolate derivative.

Molecular Structure of Complex 1. Pictured in Figure 2 is the crystallographically determined structure of tetrakisenolate **1**. The pair of trans O−Mo−O angles are ca. 150°, indicating a substantially less flattened D_{2d} core than that found by Schrock et al. in the case of $W(OAr)_4$,[5,6] where the trans O−W−O angles were 168°. The Mo−O−C angles in **1** are rather open, ranging from 145° to 150°. The M−O bond distances in **1** are similar to those found for $W(OAr)_4$, in the 1.83−1.87 Å range.

Adamantylidene cages and mesityl substituents are densely interdigitated about the central MoO_4 core and can be expected to modulate substantially the small-molecule reactivity of complex **1**.

Geometric and Electronic Structure of Complex 1. As suggested by Chisholm et al.,[2] there is the possibility that sterically demanding substituents, such as those employed in the design of **1**, might tend to favor a tetrahedral over a square-planar core geometry for $Mo(OR)_4$ complexes. To test this idea, we performed geometry optimization calculations on two models for system **1**. Model $Mo(OC[CMe_2]Ph)_4$ (**1m**) was subjected to optimization in C_2 symmetry with substituents arranged as observed in the structure of **1**. Note that **1** has a pseudo-C_2 axis that bisects the cis O1−Mo−O1′ and O2−Mo−O2′ angles. Trans O−Mo−O angles for **1m** were calculated to be 150°, and the other core structural parameters were similarly a near-perfect match with the metrical parameters observed for **1**. In addition, model $Mo(OH)_4$ (**1m′**) was geometry-optimized in D_{2d} symmetry, providing a calculated pair of trans O−Mo−O angles = 143°. These results show that $Mo(OR)_4$ systems inherently adopt a D_{2d} core geometry that is midway between tetrahedral and square planar, at least for the following choices of R: H, C[CMe_2]Ph, or C[2-Ad]Mes.

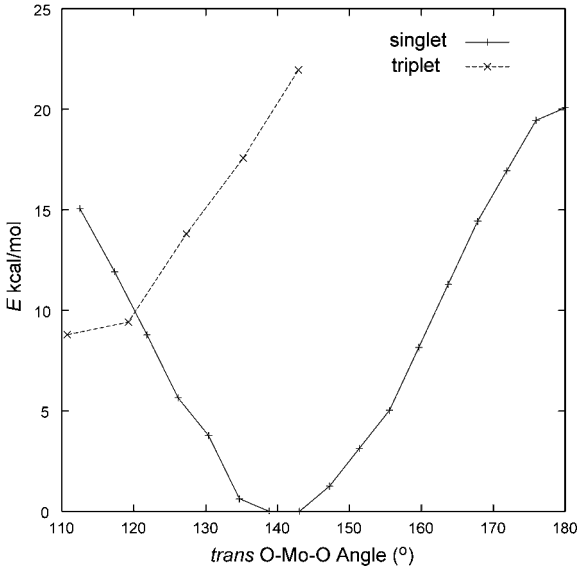

Figure 3. Relative energy of D_{2d} $^1[Mo(OH)_4]$ and $^3[Mo(OH)_4]$ calculated as a function of the trans O−Mo−O angle.

In an effort to understand the origin of the observed geometric preference, we carried out a series of constrained geometry optimizations for $Mo(OH)_4$ (**1m′**) varying the trans O−Mo−O angles from 110° (tetrahedral) to 180° (square planar), for both the singlet and the triplet electronic configurations (Figure 3). As expected, the triplet is favored as the structure approaches tetrahedral, the crossing point between the two surfaces occurring at ca. 120°. At the preferred structure of the singlet, the triplet lies higher in energy by 20 kcal mol^{-1}.

What is surprising about Figure 3 is that the energy of the singlet rises steeply at angles greater than 145°. Prior analyses based on orbital overlap have suggested that 180° should be the preferred angle for the singlet.[4] An energy partitioning analysis[10] reveals this to be not at variance with our results because, although the attractive $\Delta E_{Orbital}$ and ΔE_{Elstat} terms become more favorable respectively by −131 and −19 kcal mol^{-1} on going from 145° to 180°, the repulsive term ΔE_{Pauli} itself outpaces them, growing by +171 kcal mol^{-1} over this range. The observed intermediate geometry is therefore interpreted as a compromise between maximizing orbital interactions and minimizing Pauli repulsions in the MoO_4 core.

As can be seen from Figure 4, the HOMO for **1m** is nearly pure Mo d_{z^2} in character, while the LUMO consists of the Mo

(8) Friebolin. H. *Basic One- and Two-Dimensional NMR Spectroscopy*, 3rd ed.; VCH: Weinheim, Germany, 1998.

(9) ORTEP drawings were produced using ORTEP-3 for Windows version 1.076 (see: Farrugia, L. J. *J. Appl. Crystallogr.* **1997**, *30*, 565) in conjunction with POV-Ray for Windows version 3.5.icl.win32.

(10) Lein, M.; Szabó, A.; Kovács, A.; Frenking, G. *Faraday Discuss.* **2003**, *124*, 365−378.

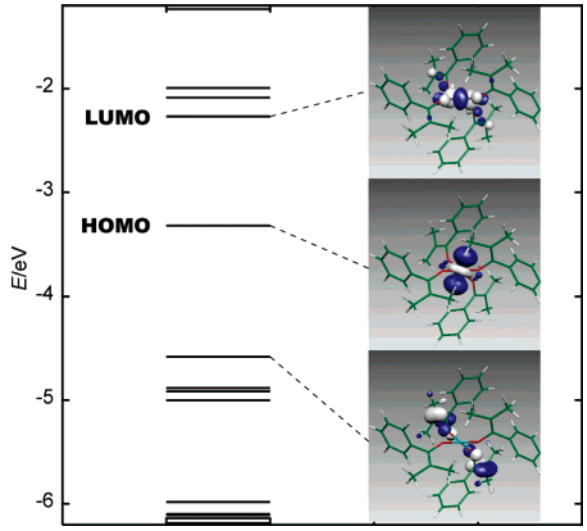

Figure 4. MO diagram for $Mo(OC[CMe_2]Ph)_4$, **1m**.

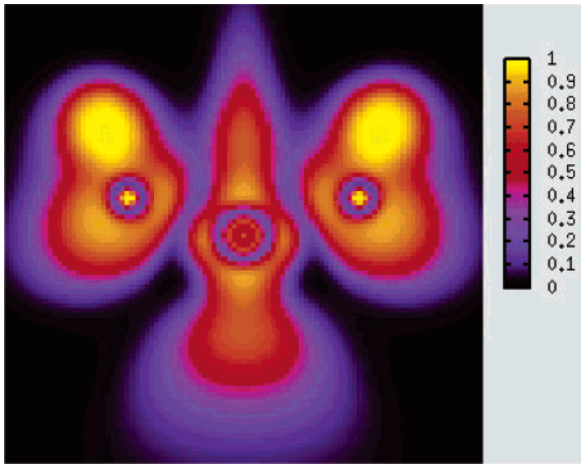

Figure 5. Plot of the ELF for **1m′** in an O−Mo−O plane with the Mo atom at the center.

$d_{x^2-y^2}$ atomic orbital augmented with π^* character with respect to the enolate oxygens. A manifold of four orbitals below the HOMO corresponds to CC π bonds; the highest-lying of these, as pictured in Figure 4, is antibonding with respect to enolate oxygen contributions.

An interesting way to visualize the electronic structure of the d^2 $Mo(OR)_4$ system is via a plot of the electron localization function (ELF, see Figure 5).[11−14] Associated with ELF values close to 1 are regions of space that correspond to bonding or lone electron pairs in the Lewis picture.[13,15,16] The shell structure of the Mo and two O nuclei in the plane of the 2D slice of Figure 5 is clearly visible, as are the O−H bonding electron pairs, the O lone pairs contained in the slice, and the Mo-based nonbonding pair of electrons. Indicative of the large ionic contribution to the Mo−O bonding is the low value of the ELF (blue contour) midway along the Mo−O vectors.

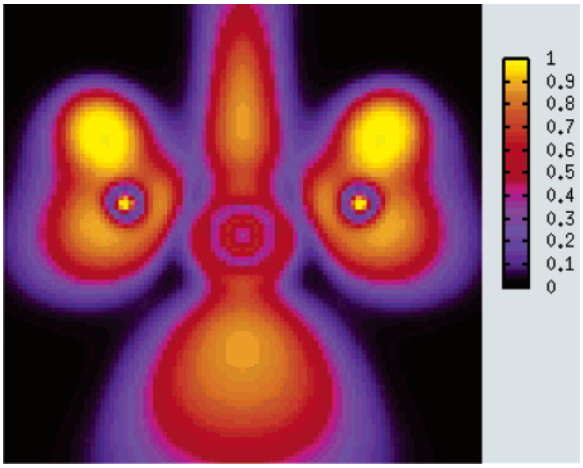

Figure 6. Plot of the ELF for D_{2d} $W(OH)_4$ in an O−W−O plane with the W atom at the center; the plot region is the same size as for $Mo(OH)_4$ in Figure 5.

The ELF also provides a clue as to why Schrock's $W(OAr)_4$ system is flatter than is our $Mo(OC[Ad]Mes)_4$ complex. Pictured in Figure 6 is a plot of the ELF for D_{2d} geometry-optimized $W(OH)_4$ (trans O−W−O angle = 148°). Striking is the contrast between Figures 5 and 6 in terms of the appearance of the metal-based lone pair. In the case of M = W, this region is strongly elongated along the *z* axis (vertical in the figures) relative to M = Mo, where values of the ELF that approach 1 are located much closer to the metal, including in the vicinity of the *xy* plane. In terms of its shape, the lone pair is a two-bladed propeller with much larger blades for tungsten than for molybdenum. This suggests that further flattening in the case of molybdenum is strongly opposed by in-plane metal−ligand Pauli repulsions. There is a correspondence with the orbital picture. In the case of tungsten, $5d_{z^2}$−6s mixing is expected to be enhanced relativistically,[17] and the enhanced mixing should lead to a diminished contribution of the $5d_{z^2}$ torus to the lone pair of the HOMO (Figure 4).

Isocyanide Binding by 1. Simple 1:1 complexation of isocyanides by homoleptic d^2 MoX_4 systems is not commonplace. For example, thiolate $Mo(S-t\text{-}Bu)_4$ reacts with *t*-BuNC (4 equiv) to extrude *tert*-butyl disulfide while forming *cis*-$(t\text{-}BuS)_2Mo(CN-t\text{-}Bu)_4$.[18] Additionally, $Mo(NMe_2)_4$ inserts 4 equiv of 2,6-dimethylphenyl isocyanide to provide $Mo(\eta^2\text{-}Me_2NCN\text{-}2,6\text{-}Me_2C_6H_3)_4$.[19] Clearly, thiolate and dimethylamide ligands both are noninnocent with respect to the isocyanide functional group, at least in the context of molybdenum(IV) chemistry. Here, our enolate supporting ligand provides a contrast, with complex **1** giving simple 1:1 binding of RNC (R = *tert*-butyl, *iso*-propyl, and 1-adamantyl).

The 1:1 isocyanide adducts **1**-CNR are obtained as brown paramagnetic compounds, the values of μ_{eff} for which, as measured by the Evans method,[20−22] are consistent with a triplet ground state. While this is consistent with either TBP or SP coordination geometries given an axially disposed isocyanide

(11) Becke, A. D.; Edgecombe, K. E. *J. Chem. Phys.* **1990**, *92*, 5397−5403.
(12) Savin, A.; Jepsen, O.; Flad, J.; Andersen, O. K.; Preuss, H.; von Schnering, H. G. *Angew. Chem., Int. Ed. Engl.* **1992**, *31*, 187−188.
(13) Savin, A.; Nesper, R.; Wengert, S.; Fassler, T. F. *Angew. Chem., Int. Ed. Engl.* **1997**, *36*, 1808−1832.
(14) Burdett, J. K. *New J. Chem.* **1997**, *21*, 289−299.
(15) A general introduction to ELF can be found at the ELF home page: http://www.cpfs.mpg.de/ELF.
(16) Lewis, G. N. *J. Am. Chem. Soc.* **1916**, *38*, 762−785.
(17) Pyykkö, P. *Chem. Rev.* **1988**, *88*, 563−594.
(18) Kamata, M.; Yoshida, T.; Otsuka, S.; Hirotsu, K.; Higuchi, T. *J. Am. Chem. Soc.* **1981**, *103*, 3572−3574.
(19) Chisholm, M. H.; Hammond, C. E.; Ho, D.; Huffman, J. C. *J. Am. Chem. Soc.* **1986**, *108*, 7860−7861.
(20) Evans, D. F. *J. Chem. Soc.* **1959**, 2003−2005.
(21) Crawford, T. H.; Swanson, J. *J. Chem. Educ.* **1971**, *48*, 382−386.
(22) Sur, S. K. *J. Magn. Reson.* **1989**, *82*, 169−173.

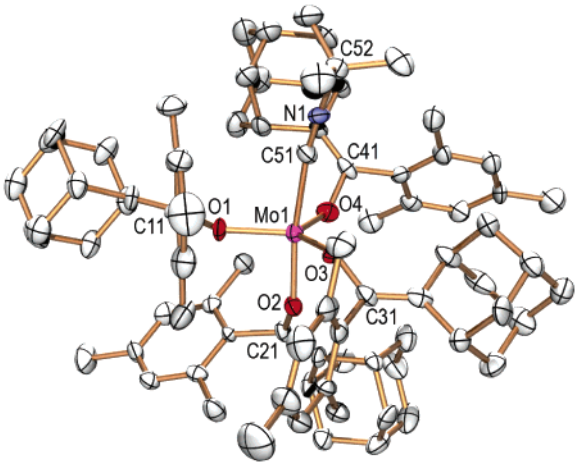

Figure 7. ORTEP[9] representation of complex **1**-CN−*t*-Bu with ellipsoids at the 50% probability level. Selected interatomic distances (Å) and angles (deg): Mo1−C51, 2.228(9); N1−C51, 1.124(9); N1−C52, 1.486(10); Mo1−O1, 1.895(5); Mo1−O2, 1.972(5); Mo1−O3, 1.894(5); Mo1−O4, 1.897(5); C51−N1−C52, 173.9(8).

ligand, the geometry observed by single-crystal X-ray diffraction for **1**-CN−*t*-Bu (Figure 7) is the TBP form. This is reminiscent of the TBP structure of $(HNMe_2)Mo(O\text{-}1\text{-}adamantyl)_4$ described by Wilkinson as having an axial dimethylamine ligand.[23] As can be seen in the caption to Figure 7, the Mo1−O2 bond (trans to the isocyanide ligand) is longer by ca. 0.08 Å than are the equatorially disposed Mo−O bonds. The Mo−C bond length of 2.228(9) Å is longer than observed for either of the molybdenum(III) mono- or bis-isocyanide adducts (*t*-BuNC)-$Mo(N[t\text{-}Bu]Ar)_3$ (1.936(6) Å) and $(1\text{-}AdNC)_2Mo(N[i\text{-}Pr]Ar)_3$ (2.135(11) and 2.083(11) Å).[24]

Reaction of Complex 1 with *dbabh*CN. Methods for introducing the cyanoimide ligand (NCN^{2-}) into the coordination sphere of metal complexes are currently emerging. An example includes the reaction of 2 equiv of the parent cyanamide, H_2NCN, with *trans*-$Mo(dppe)_2(N_2)_2$ to produce the bis-cyanoimide molybdenum(IV) derivative *trans*-$Mo(dppe)_2(NCN)_2$ together with evolution of $2H_2$ and $2N_2$.[25] Simple salt elimination has also been used; μ-NCN complexes of tungsten and cobalt have been prepared using $K_2(NCN)$ as the cyanoimide source.[26] The possibility that cyanoimide may serve as a building block analogous to cyanide in the preparation of extended solids with interesting magnetic properties[27−29] sparked recently a synthesis of a tetranuclear iridium cubane complex bearing μ_3-NCN units at four cube vertices: $(Cp^*Ir\{\mu_3\text{-}NCN\})_4$.[30] Cyanoimide introduction in the latter case was via Na(NCNH).

We synthesized recently (from the corresponding *N*-bromo compound[31]) an organic cyanamide dubbed *dbabh*CN (Scheme 1), that serves as a source of the neutral NCN unit.[32] Reducing metals can accept NCN from *dbabh*CN with 2e oxidation of the acceptor and extrusion of neutral anthracene. Thus, *dbabh*CN affords a smooth redox delivery of NCN in homogeneous organic media. Examples of NCN complexes synthesized using *dbabh*CN are the μ-cyanoimide complexes $(\mu\text{-}NCN)\{M(N[R]\text{-}Ar)_3\}_2$, where M = U, V, and Mo. The reactions used to prepare the latter complexes involved simple addition of *dbabh*CN to a solution containing 2 equiv of $M(N[R]Ar)_3$ (THF adduct for M = U). Anthracene formed smoothly, and the bimetallic complexes were presumed formed via capping off of the putative, unobserved terminal mononuclear metal(V) cyanoimide complexes, $(NCN)M(N[R]Ar)_3$. The latter remain interesting as synthetic targets because of their terminal functionality combined with redox activity.

Scheme 1. Reaction of **1** with *dbabh*CN To Provide **1**-NCN and Anthracene

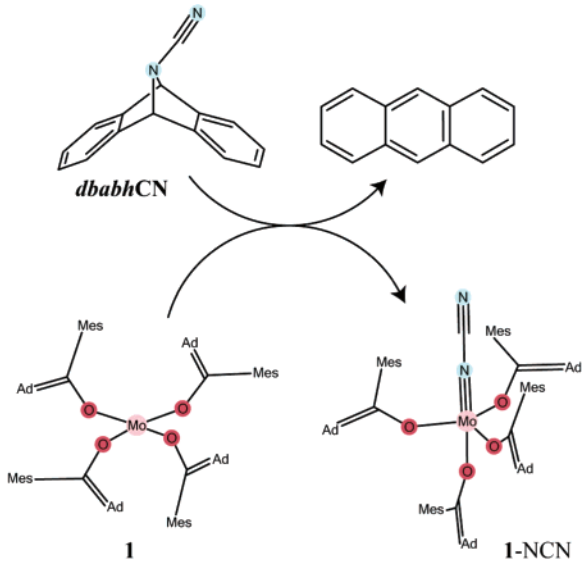

It is presumed that the Mo(IV)/Mo(VI) two-electron redox couple will be available for many of the reactions of **1**. This would be very much in line with Chisholm's study of $Mo(O\text{-}t\text{-}Bu)_4$ with molecular oxygen to provide $OMo(O\text{-}t\text{-}Bu)_4$ as a yellow liquid.[33] The related volatile, yellow crystalline compound $OMo(OC[CF_3]_3)_4$ has been characterized structurally by X-ray diffraction methods and found to be a trigonal bipyramid with an equatorial molybdyl group.[34] The structure of $OMo(OC[CF_3]_3)_4$ has alternatively been described as a square pyramid with an apical oxo ligand.[33] The structure of $OMo(OTeF_5)_4$ is similar.[35] On the other hand, $OMo(3,6\text{-}DBCat)_2$ is found to be dimeric in the solid state by virtue of bridging catecholate oxygens.[36] For R = Me, Et, *i*-Pr, or CH_2CH_2OMe, it has been shown by conductometric titration that $OMo(OR)_4$ is dimeric in alcoholic solution.[37] Similarly, $OW(OR)_4$ com-

(23) Bochmann, M.; Wilkinson, G.; Young, G. B.; Hursthouse, M. B.; Malik, K. M. A. *J. Chem. Soc., Dalton Trans.* **1980**, 901−910.
(24) Stephens, F. H.; Figueroa, J. S.; Cummins, C. C.; Kryatova, O. P.; Kryatov, S. V.; Rybak-Akimova, E. V.; McDonough, J. E.; Hoff, C. D. *Organometallics* **2004**, *23*, 3126−3138.
(25) Cunha, S. M. P. R. M.; da Silva, M. F. C. G.; Pombeiro, A. J. L. *J. Chem. Soc., Dalton Trans.* **2002**, 1791−1799.
(26) Cao, R.; Tatsumi, K. *Chem. Commun.* **2002**, 2144−2145.
(27) Entley, W. R.; Girolami, G. S. *Science* **1995**, *268*, 397−400.
(28) Verdaguer, M.; Bleuzen, A.; Marvaud, V.; Vaissermann, J.; Seuleiman, M.; Desplanches, C.; Scuiller, A.; Train, C.; Garde, R.; Gelly, G.; Lomenech, C.; Rosenman, I.; Veillet, P.; Cartier, C.; Villain, F. *Coord. Chem. Rev.* **1999**, *190−192*, 1023−1047.
(29) Dunbar, K. R.; Heintz, R. A. *Prog. Inorg. Chem.* **1997**, *45*, 283−391.
(30) Tanabe, Y.; Kuwata, S.; Ishii, Y. *J. Am. Chem. Soc.* **2002**, *124*, 6528−6529.
(31) Carpino, L. A.; Padykula, R. E.; Barr, D. E.; Hall, F. H.; Krause, J. G.; Dufresne, R. F.; Thoman, C. J. *J. Org. Chem.* **1988**, *53*, 2565−2572.
(32) Mindiola, D. J.; Tsai, Y.-C.; Hara, R.; Chen, Q.; Meyer, K.; Cummins, C. C. *Chem. Commun.* **2001**, 125−126.
(33) Chisholm, M. H.; Folting, K.; Huffman, J. C.; Kirkpatrick, C. C. *Inorg. Chem.* **1984**, *23*, 1021−1037.
(34) Johnson, D. A.; Taylor, J. C.; Waugh, A. B. *J. Inorg. Nucl. Chem.* **1980**, *42*, 1271−1275.
(35) Turowsky, L.; Seppelt, K. *Z. Anorg. Allg. Chem.* **1990**, *590*, 23−36.
(36) Liu, C.-M.; Nordlander, E.; Schmeh, D.; Shoemaker, R.; Pierpont, C. G. *Inorg. Chem.* **2004**, *43*, 2114−2124.
(37) Turova, N. Ya.; Kessler, V. G.; Kucheiko, S. I. *Polyhedron* **1991**, *10*, 2617−2628.

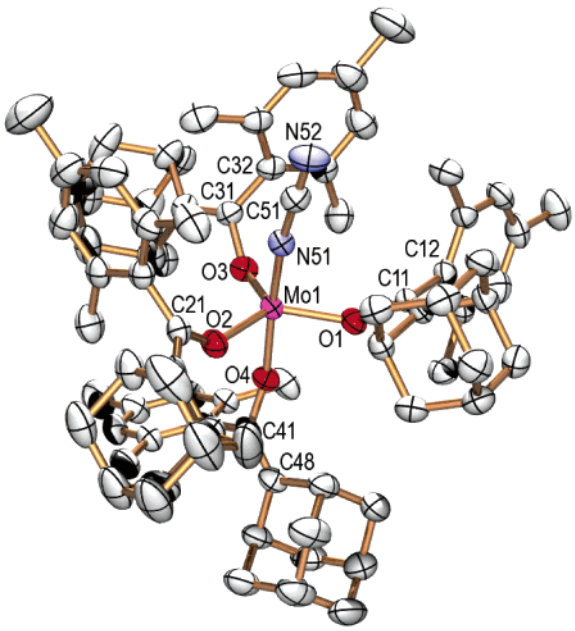

Figure 8. ORTEP[9] representation of complex **1**-NCN with ellipsoids at the 50% probability level. Selected interatomic distances (Å) and angles (deg): Mo1−N51, 1.792(3); N51−C51, 1.306(6); C51−N52, 1.155(6); C51−N51−Mo1, 171.7(3); N52−C51−N51, 179.2(6); N51−Mo1−O4, 173.62(13).

plexes are dimeric with alkoxide bridges both in solution and in the solid state for R = Me, Et, *i*-Pr, and *cyclo*-C_6H_{11}.[38] The phenylimido complex PhNMo[*p*-*t*-Bu-calix[4]] obtained by azobenzene cleavage is dimeric in the solid state with bridging phenolate residues;[39] it is noteworthy that the latter study was carried out with the intent of elucidating the reactivity of molybdenum(IV)/d^2 in a quasi-planar coordination environment and that Floriani implicates a very reactive Mo^{IV}-d^2-carbenoid (analogous to **1**) in the azobenzene cleavage chemistry.

In accord with our expectation that **1** should be able to accept an oxo or nitrene moiety along with conversion to molybdenum-(VI), we find that **1** reacts smoothly according to Scheme 1 with *dbabh*CN. In contrast to the reported yellow color for tetraalkoxymolybdenum oxo systems,[33] we find the cyanoimido complex **1**-NCN to be purple. Perhaps there is a structural basis for the color difference. Structural characterization (Figure 8) of **1**-NCN shows that this system adopts a TBP structure (apical NCN) with an N51−Mo1−O4 trans angle of 173.62(13)°. This is in stark contrast with known mononuclear (oxo/imido)M-$(OR)_4$ (M = Mo, W) systems that lack a ligand trans to the metal−oxygen/nitrogen multiple bond. Complex **1**-NCN is fluxional in solution such that a single set of enolate ligand resonances is observed by ^{1}H NMR spectroscopy.

Having observed the spontaneous nature of NCN transfer according to eq 1 in Table 1, a very interesting question arises as to the thermochemistry of such a process. Because NCN transfer is a new type of atom/group-transfer process, one which we expect may be profitably compared with more established processes such as oxo transfer,[40] we undertook the estimation of the relevant bond strengths using DFT methods.

Geometry optimization was performed for each of the molecules in eqs 2−4 (Table 1). The calculations on **1m** and

Table 1.

reaction	ΔH_{rxn} (kcal mol^{-1})	eq
1 + *dbabh*CN → **1**-NCN + $C_{14}H_{10}$		1
1m + *dbabh*CN → **1m**-NCN + $C_{14}H_{10}$	−77	2
*dbabh*CN → $C_{14}H_{10}$ + ^{3}[NCN]	+27	3
^{3}[NCN] + **1m** → **1m**-NCN	−104	4
PMe_3 + *dbabh*CN → $NCNPMe_3$ + $C_{14}H_{10}$	−47	5
$NCNPMe_3$ → PMe_3 + ^{3}[NCN]	+74	6

(η^1-NCN)Mo(OC[CMe_2]Ph)$_4$ (**1m**-NCN) took as starting points models derived from the crystallographically determined coordinates for **1** and **1**-NCN. Optimization of the *dbabh*CN structure (Scheme 1) assumed only C_s symmetry, while that for anthracene ($C_{14}H_{10}$) took advantage of D_{2h} symmetry. The neutral NCN molecule was calculated in its triplet ground state,[41] signified by the formula ^{3}[NCN], employing the spin-unrestricted formalism (two spin α electrons in excess of spin β) and $D_{\infty h}$ point symmetry. The key findings, listed in Table 1, pertain to ΔH_{rxn} for NCN transfer. Overall, the transfer of neutral NCN from anthracene to model molybdenum tetrakis-enolate complex **1m** is predicted to be enthalpically favorable by 77 kcal mol^{-1}. Because *dbabh*CN was designed with the built-in notion of anthracene, a stable aromatic leaving group, being able to serve as a "launch pad" for neutral NCN, we expected that the favorable nature of eq 1 might be due in large part to the low affinity of anthracene for NCN. This is expressed according to eq 3, the dissociation of *dbabh*CN into anthracene and ^{3}[NCN], enthalpically unfavorable by only 27 kcal mol^{-1}. Contrast this with the strong affinity of **1m** for NCN, expressed in eq 4 by the −104 kcal mol^{-1} heat of reaction of ^{3}[NCN] with **1m** to provide **1m**-NCN. Thus, we may interpret reaction 1 very much as it was intended, with *dbabh*CN as a potent NCN donor, and homoleptic enolate complex **1** as an enthusiastic acceptor.

To put these numbers into context, we calculated the affinity of a representative phosphine, PMe_3, for the NCN group (reactions 5 and 6 in Table 1). The P−N bond dissociation enthalpy is calculated (eq 6) to be +74 kcal mol^{-1}, and thus the exothermicity for NCN abstraction from *dbabh*CN by PMe_3 is calculated to be 47 kcal mol^{-1}. The latter value is 30 kcal mol^{-1} less than the associated value for eq 2, revealing in this context the profoundly superior reducing capacity of the d^2 metal fragment as compared with phosphorus(III). Note that the calculated P−N bond strength of 74 kcal mol^{-1} for $NCNPMe_3$ is substantially less than that (127.4 kcal mol^{-1}) calculated recently for $HNPMe_3$,[42] presumably due to the stabilization of ^{3}[NCN] relative to nitrene.

The foregoing analysis of bond strengths is not meant as an assertion that we invoke ^{3}[NCN] as an intermediate in the group-transfer process. This ground state for linear $D_{\infty h}$ NCN is merely a computational expedient that permits assessment of relative contributions to the overall reaction enthalpy. Coordination of the terminal *dbabh*CN nitrogen atom to the Mo center of **1**, followed by anthracene extrusion, is our working hypothesis for the mechanism of eq 1.

(38) Clegg, W.; Errington, R. J.; Kraxner, P.; Redshaw, C. *J. Chem. Soc., Dalton Trans.* **1992**, 1431−1438.
(39) Guillemot, G.; Solari, E.; Scopelliti, R.; Floriani, C. *Organometallics* **2001**, *20*, 2446−2448.
(40) Holm, R. H.; Donahue, J. P. *Polyhedron* **1993**, *12*, 571−589.
(41) Perić, M.; Krmar, M.; Radić-Perić, J.; Hanrath, M. *J. Mol. Spectrosc.* **2000**, *204*, 226−234.
(42) Lu, W. C.; Sun, C. C. *THEOCHEM* **2002**, *593*, 1−7.

Conclusions

Complex **1** provides for the first time a structurally characterized example of a $Mo(OR)_4$ system. The coordination geometry observed for **1** is at the midpoint between limiting tetrahedral and square-planar geometries, along a D_{2d} flattening coordinate. Computational results show that the observed structure is an inherent electronic compromise between favorable orbital interactions and unfavorable Pauli repulsions as the structure is flattened to trans O−Mo−O angles greater than ca. 150°. The observed coordination geometry is not a consequence of bulky ligand substituents. Plots of the ELF for $M(OH)_4$ systems (M = Mo and W) provide a graphic depiction of the metal-based lone pair of electrons, which in the case of M = W is extended far from the metal revealing why Pauli repulsions in the case of M = W are mitigated and permit a structure closer to square planar. It is found that complex **1** makes simple 1:1 isocyanide adducts; the *t*-BuNC adduct is trigonal bipyramidal with axial *t*-BuNC. Complex **1** reacts with NCN donor *dbabh*CN giving smooth conversion to a rare terminal cyanoimide complex **1**-NCN, the structural characterization of which revealed it to be trigonal bipyramidal with axial cyanoimide. The latter group-transfer reaction is calculated to be very exothermic (ΔH_{rxn} = 77 kcal mol^{-1}) as a consequence of the thermodynamic instability of *dbabh*CN in concert with the formation of a strong cyanoimide Mo−N bond (ca. 104 kcal mol^{-1}).

It is our hope that the fascinating structure and potent two-electron reactivity available to $Mo(OR)_4$ will stimulate further research into its chemistry.

Computational Details

All DFT calculations were carried out using the Amsterdam Density Functional (ADF) program package,[43,44] version 2002.03.[45] The local exchange-correlation potential of Vosko et al.[46] (VWN) was augmented self-consistently with gradient-corrected functionals for electron exchange according to Becke,[47] and electron correlation according to Perdew.[48,49] This nonlocal density functional is termed BP86 in the literature and has been shown to give excellent results both for the geometries and for the energetics of transition metal systems.[50] Relativistic effects were included using the zero-order regular approximation (ZORA).[51,52] The basis set used was the all-electron ADF ZORA/TZ2P (triple-ζ with two polarization functions) basis.

Data for the ELF plots in Figures 5 and 6 were generated by postprocessing an ADF calculation using the DGRID/BASIN program[53] and were plotted using GNUPLOT.[54,55] Orbital pictures as in Figure 4 were generated using MOLEKEL,[56,57] to process the ADF results.

(43) te Velde, G.; Bickelhaupt, F. M.; van Gisbergen, S. J. A.; Fonseca Guerra, C.; Baerends, E. J.; Snijders, J. G.; Ziegler, T. *J. Comput. Chem.* **2001**, *22*, 931−967.
(44) Fonseca Guerra, C.; Snijders, J. G.; te Velde, G.; Baerends, E. J. *Theor. Chem. Acc.* **1998**, *99*, 391−403.
(45) *ADF2002.03*; SCM, Theoretical Chemistry, Vrije Universiteit, Amsterdam, The Netherlands, http://www.scm.com.
(46) Vosko, S. H.; Wilk, L.; Nusair, M. *Can. J. Phys.* **1980**, *58*, 1200−1211.
(47) Becke, A. *Phys. Rev. A* **1988**, *38*, 3098−3100.
(48) Perdew, J. P. *Phys. Rev. B* **1986**, *34*, 7406−7406.
(49) Perdew, J. P. *Phys. Rev. B* **1986**, *33*, 8822−8824.
(50) See, for example: Deng, L.; Schmid, R.; Ziegler, T. *Organometallics* **2000**, *19*, 3069−3076.
(51) van Lenthe, E.; Baerends, E. J.; Snijders, J. G. *J. Chem. Phys.* **1993**, *99*, 4597−4610.
(52) van Lenthe, E. The ZORA Equation. Thesis, Vrije Universiteit Amsterdam, Netherlands, 1996.
(53) Kohout, M. *DGRID/BASIN*; Version 2.4, 2002.
(54) Williams, T.; Kelley, C.; et al. *GNUPLOT*, version 3.8k; Patchlevel 2, 2003.
(55) Moore, B. G. *J. Chem. Educ.* **2000**, *77*, 785−789.
(56) Flukiger, P.; Luthi, H. P.; Portmann, S.; Weber, J. *MOLEKEL 4.3*; Swiss Center for Scientific Computing, Manno, 2000; http://www.cscs.ch/molekel.
(57) Portmann, S.; Lüthi, H. P. *Chimia* **2000**, *54*, 766−769.

Experimental Section

See ref 7 for a description of general procedures.

Preparation of Mo(OC[Ad]Mes)$_4$, 1. To a thawing slurry of K(OC[Ad]Mes) (9.000 g, 28.1 mmol, 4.1 equiv) in 1,2-dimethoxyethane was added $MoCl_4(THF)_2$ (2.616 g, 6.85 mmol) with magnetic stirring. The reaction mixture took on the appearance of a dark green slurry. After 16 h at 25 °C, the reaction mixture was filtered through Celite. The filter cake was further rinsed with 10 mL of diethyl ether. The filtrate contained very little **1**, together with free ketone ligand and another organic byproduct believed to arise via unsymmetrical oxidative coupling of the enolate ligand. The filtrate was discarded. The filter cake was then extracted by stirring with 350 mL of toluene. The green extract was filtered and concentrated to ca. 30 mL. To the concentrate was added 10 mL of diethyl ether, whereupon the mixture was stored at −40 °C overnight. This led to deposition of **1** as a yellow-green precipitate, which was collected by filtration (37% yield in two crops, 3.082 g, 2.52 mmol). Yellow single crystals of **1** for the X-ray diffraction experiment were obtained after several days from a dilute ether solution cooled to −40 °C. Anal. Calcd for $C_{80}H_{100}O_4Mo$: C, 78.66; H, 8.25. Found: C, 78.53; H, 8.31. ^{1}H NMR (500 MHz, C_6D_6): δ = 1.6−1.9 (m, 24H, adamantylidene), 2.26 (s, 4H, allylic H), 2.45 (s, 12H, *para*-CH_3), 2.5−2.7 (m, 16H, adamantylidene), 2.69 (s, 24H, *ortho*-CH_3), 2.92 (d, J = 11.5 Hz, 8H, adamantylidene), 5.16 (bs, 4H, allylic H as determined by ^{1}H−^{1}H COSY and HETCOR experiments), 7.11 (s, 8H, 2,4,6-C$_6H_2$Me$_3$). ^{13}C{^{1}H} NMR (C_6D_6, assignments aided by DEPT, HETCOR, and COSY experiments): δ = 21.09 (*ortho*-*C*H$_3$), 27.32 (*para*-*C*H$_3$), 29.32 (allylic *C*H), 29.65 (*C*H), 38.09 (*C*H$_2$), 45.44 (*C*H$_2$), 49.81 (*C*H$_2$), 49.94 (allylic *C*H), 100.92 (enolate O−C=*C*), 129.31 (mesityl *C*H), 138.27 (mesityl *C*), 144.79 (mesityl *C*), 170.44 (mesityl *C*), 176.13 (enolate O−*C*=C). IR (C_6D_6, cm^{-1}): 1068 (vs, CO), 2849 (m, CH), 2910 (s, CH).

Preparation of Isocyanide Adducts (RNC)Mo(OC[Ad]Mes)$_4$; R = *t*-Bu, *i*-Pr, and 1-Adamantyl. Described in detail is the preparation of **1**-CN−*t*-Bu; the other adducts were obtained similarly. Tetrakis-enolate **1** (0.054 g, 0.0442 mmol) was slurried in 4 mL of Et_2O, and the slurry was frozen. Excess *t*-BuNC (0.037 g, 0.445 mmol, 10.1 equiv) was dissolved in 2 mL of Et_2O, and the solution was frozen. The thawing *t*-BuNC solution was subsequently added to the thawing slurry of **1**, and the reaction mixture was stirred as it warmed to room temperature. A reddish-brown solution formed as yellow-green **1** dissolved. After 15 min, the reaction mixture was filtered, and the filtrate was concentrated to dryness. The residue so obtained was dissolved in 0.5 mL of toluene and layered beneath 2 mL of Et_2O in a scintillation vial, which then was stored at −40 °C. After 1 week, brown, single crystals of **1**-CN−*t*-Bu were collected by filtration in 57% yield (0.033 g, 0.0251 mmol). An X-ray structural study was conducted on one of the single crystals.

^{1}H NMR (300 MHz, C_6D_6): δ = −0.82 (bs), 0.51 (bs), 1.73 (bs), 2.14 (s), 3.00 (s), 3.83 (bs), 4.02 (bs), 6.46 (bs), 7.59 (bs), 8.20 (bs), 8.66 (bs), 11.61 (bs), 16.01 (bs). μ_{eff} (Evans' method, C_6D_6, 294 K): 2.92 μ_B. IR (C_6D_6, cm^{-1}): 1058 (s, C−O), 1065 (s, C−O), 2157 (m, CN), 2909 (s, CH). Anal. Calcd for $C_{85}H_{109}O_4NMo$: C, 78.25; H, 7.72; N, 1.07. Found: C, 78.03; H, 7.65; N, 1.10.

Data for 1-CN−1-Adamantyl. Quantities employed: AdNC, 0.021 g, 0.130 mmol, 1.05 equiv; **1**, 0.152 g, 0.124 mmol. Isolated yield: 74% (0.127 g, 0.0918 mmol). ^{1}H NMR (500 MHz, C_6D_6): δ = −5.84 (bs), −0.91 (bs), 0.39 (bs), 0.55 (bs), 0.98 (bs), 2.07 (s), 3.75 (bs), 4.05 (bs), 6.46 (bs), 7.34 (bs), 8.19 (bs), 8.54 (bs), 11.43 (bs), 11.88 (bs), 11.96(bs), 16.52 (bs). μ_{eff} (Evans' method, C_6D_6, 292 K): 2.92 μ_B. IR (C_6D_6, cm^{-1}): 1059 (s, C−O), 1066 (s, C−O), 2157 (m, CN), 2910 (s, CH). Anal. Calcd for $C_{91}H_{115}O_4NMo$: C, 79.04; H, 8.38; N, 1.01. Found: C, 79.12; H, 8.31; N, 0.98.

Data for 1-CN−*i*-Pr. Quantities employed: *i*-PrNC, 0.010 g, 0.145 mmol, 1.7 equiv; **1**, 0.103 g, 0.0842 mmol. Isolated yield: 23% (0.025 g, 0.0194 mmol). ^{1}H NMR (500 MHz, C_6D_6): δ = −0.89 (bs), −0.79

(bs), 0.35 (bs), 0.66 (m), 0.89 (bs), 2.61 (bs), 3.09 (s), 3.59 (bs), 3.86 (bs), 4.31 (bs), 4.98 (bs), 6.72 (bs), 6.88 (bs), 7.33 (bs), 7.87 (bs), 9.94 (bs), 11.36 (bs), 12.17 (bs), 15.77 (bs), 16.83(bs). μ_{eff} (Evans' method, C_6D_6, 294 K): 2.26 μ_B. IR (C_6D_6, cm^{-1}): 1058 (s, C−O), 1067 (s, C−O), 2142 (w, CN), 2173 (m, CN), 2907 (vs, CH). Anal. Calcd for $C_{84}H_{107}O_4NMo$: C, 78.17; H, 8.35; N, 1.09. Found: C, 77.96; H, 8.29; N, 1.06.

Preparation of 1-NCN. *dbabh*CN (0.020 g, 0.0916 mmol, 1.1 equiv) was slurried in Et_2O (2 mL), and the slurry was frozen. Complex **1** (0.107 g, 0.0873 mmol) was slurried in Et_2O (4 mL), and this slurry was frozen as well. The vessels containing the frozen slurries were removed from the glovebox cold well and permitted to begin to thaw. The thawing *dbabh*CN slurry was added to the thawing slurry of **1**, and the reaction mixture was stirred as it warmed to room temperature. A dark purple solution formed within 10 min as yellow-green **1** dissolved. After 30 min, the solvent was removed from the reaction mixture under reduced pressure, after which the residue was extracted with 2 × 2 mL of hexane and the extract filtered to remove some anthracene. The filtrate was dried again, and the purple residue was slurried in ca. 2 mL of pentane and frozen. After the frozen purple slurry began thawing, filtration was carried out to remove most of the remaining anthracene. The filter cake also was rinsed with 1 mL of thawing pentane. The filtrate was then dried in vacuo, the residue was dissolved in ca. 0.5 mL of pentane, the solution was filtered, and the filtrate was stored at −40 °C. Purple crystals were collected in 73% yield in three crops (0.080 g, 0.0634 mmol). Purple single crystals of **1**-NCN were grown out of an *n*-pentane solution for X-ray structural analysis.

^{1}H NMR (500 MHz, C_6D_6): δ = 1.6−2.2 (m, 52H, adamantyl), 2.23 (s, 12H, *p*-Me), 2.30 (s, 24H, *o*-Me), 3.29 (bs, 4H, allylic H), 6.84 (s, 8H, aryl-H).

^{13}C NMR (500 MHz, C_6D_6, {^{1}H}, assignments aided by DEPT): δ = 21.31 (*o*-CH_3), 21.63 (*p*-CH_3), 29.14 (CH), 31.32 (allylic CH), 34.00 (allylic CH), 37.67 (CH_2), 39.79 (CH_2), 39.95 (CH_2), 100.49 (enolate O−C═*C*), 129.25 (aryl CH), 130.79 (NCN), 134.07 (aryl), 137.44 (aryl), 137.64 (aryl), 152.50 (enolate O−*C*═C).

IR (C_6D_6, cm^{-1}): 731 (m), 1045 (s, C−O), 1294 (m, N−C≡N), 2083 (m, N−C≡N), 2850 (m, C−H), 2912 (vs, C−H), 2956 (m, C−H).

Anal. Calcd for $C_{81}H_{100}O_4N_2Mo$: C, 77.11; H, 7.99; N, 2.22. Found: C, 76.85; H, 8.11; N, 2.16.

Crystallographic Structure Determinations. The X-ray data collections were carried out on a Siemens Platform three-circle diffractometer mounted with a CCD detector and outfitted with a low-temperature, nitrogen-stream aperture. The structures were solved using direct methods, in conjunction with standard difference Fourier techniques, and were refined by full-matrix least-squares procedures. A summary of cyrstallographic data is given in Table 2. The systematic absences in the diffraction data were uniquely consistent with the assigned monoclinic space groups of *P*2/*n*, *P*2$_1$/*c*, and *C*2/*c* for **1**, **1**-CN−*t*-Bu, and **1**-NCN, respectively. These choices led to chemically sensible and computationally stable refinements. SADABS absorption correction was applied to all structures. All hydrogen atoms were placed in calculated positions (d_{C-H} = 0.96 Å). Complexes **1** and **1**-CN−*t*-Bu cocrystallized with one and two well-behaved molecules of diethyl ether, respectively. Complex **1**-NCN cocrystallized with several disordered molecules of ethyl ether, of which two were reasonably modeled and refined isotropically without hydrogen atoms. The remaining peaks in the electron density map could not be reasonably modeled as discrete molecules. The crystallographic routine SQUEEZE[58,59] was employed and found a total of 120 electrons in a solvent-accessible void area of 3627.0 Å^3 (20.5% of unit cell volume), corresponding to 2.85 additional molecules of diethyl ether per unit cell (0.35 additional molecules of diethyl ether per molecule of **3**). The final stages of refinement for complex **3** were performed against the solvent-free (for substoichiometric diethyl ether) reflection file obtained from SQUEEZE and resulted in significant improvements of the final residual values. All software for diffraction data processing and crystal-structure solution and refinement are contained in the SHELXTL (v6.14) program suite (G. Sheldrick, Bruker XRD, Madison, WI).

Table 2. Crystallographic Data for Complexes **1**, **1**-CN−*t*-Bu, and **1**-NCN

	1·(Et_2O)	**1**-CN–*t*-Bu·(Et_2O)$_2$	**1**-NCN·(Et_2O)$_{1.5}$
formula	$C_{84}H_{110}MoO_5$	$C_{93}H_{129}MoNO_6$	$C_{87}H_{100}MoN_2O_{5.50}$
fw	1295.66	1452.91	1357.63
space group	*P*2/*n*	*P*2$_1$/*c*	*C*2/*c*
a, Å	13.7244(10)	13.7807(11)	34.554(4)
b, Å	12.8123(9)	22.8234(17)	20.891(2)
c, Å	21.4443(14)	26.558(2)	24.730(3)
α, deg	90	90	90
β, deg	105.9970(10)	101.402(2)	99.320(2)
γ, deg	90	90	90
V, Å^3	3624.8(4)	8188.2(11)	17 616(3)
Z	2	4	8
D(calcd), g/cm^3	1.187	1.179	1.024
μ (Mo Kα), mm^{-1}	0.232	0.213	0.194
temp, K	183(2)	183(2)	183(2)
radiation	Mo Kα (λ = 0.71073 Å)		
R(*F*), %[a]	0.0584	0.0862	0.0572
R_w(*F*), %[a]	0.0660	0.1760	0.0818

[a] Quantity minimized = $R_w(F^2) = \sum[w(F_o^2 - F_c^2)^2]/\sum[(wF_o^2)^2]^{1/2}$; $R = \sum\Delta/\sum(F_o)$, $\Delta = |(F_o - F_c)|$, $w = 1/[\sigma^2(F_o^2) + (aP)^2 + bP]$, $P = [2F_c^2 + \mathrm{Max}(F_o,0)]/3$.

Acknowledgment. This paper is dedicated to the memory of Professor Ian P. Rothwell. For helpful discussions, C.C.C. thanks Professors Peter T. Wolczanski, Richard R. Schrock, and Eric A. Maatta. C.C.C. further wishes to thank Dr. M. Kohout for his very helpful comments on the use of ELF in this manuscript. H.S.S. thanks the Public Service Commission (Singapore) for an OMS scholarship. We are grateful for funding from the U.S.A. National Science Foundation (CHE-0316823).

Supporting Information Available: Text-only atom coordinate files in xyz format for all geometry-optimized structures. This material is available free of charge via the Internet at http://pubs.acs.org.

JA0472533

(58) van der Sluis, P.; Spek, A. L. *Acta Crystallogr.* **1990**, *A46*, 194−201.
(59) Spek, A. L. *Acta Crystallogr.* **1990**, *A46*, C34−C34.